

# Style Content Decomposition-based Data Augmentation for Domain Generalizable Medical Image Segmentation

Zhiqiang Shen<sup>1,2,4</sup>

XXSZQYY@GMAIL.COM

Peng Cao<sup>1,2</sup>

Jinzhu Yang<sup>1,2</sup>

<sup>1</sup> School of Computer Science and Engineering, Northeastern University, Shenyang, China.

<sup>2</sup> Key Laboratory of Intelligent Computing in Medical Image, Ministry of Education, Northeastern University, Shenyang, China

Osmar R. Zaiane<sup>3</sup>

<sup>3</sup> Alberta Machine Intelligence Institute, University of Alberta, Edmonton, Canada

Zhaolin Chen<sup>4,5</sup>

<sup>4</sup> Department of Data Science & AI, Faculty of Information Technology, Monash University, Melbourne, Australia

<sup>5</sup> Monash Biomedical Imaging, Monash University, Melbourne, Australia

## Abstract

Due to domain shifts across diverse medical imaging modalities, learned segmentation models often suffer significant performance degradation during deployment. We posit that these domain shifts can generally be categorized into two main components: 1) **”style” shifts**, referring to global disparities in image properties such as illumination, contrast, and color; and 2) **”content” shifts**, which involve local discrepancies in anatomical structures. To address the domain shifts in medical image segmentation, we first factorize an image into style codes and content maps, explicitly modeling the “style” and “content” components. Building on this, we introduce a **Style-Content** decomposition-based data **augmentation** algorithm (StyCona), which performs augmentation on both the global style and local content of source-domain images, enabling the training of a well-generalized model for domain generalizable medical image segmentation. StyCona is a simple yet effective plug-and-play module that substantially improves model generalization without requiring additional training parameters or modifications to segmentation model architectures. Experiments on cardiac magnetic resonance imaging and fundus photography segmentation tasks, with single and multiple target domains respectively, demonstrate the effectiveness of StyCona and its superiority over state-of-the-art domain generalization methods. The code is available at <https://github.com/Senyh/StyCona>.

**Keywords:** Medical Image Segmentation, Domain Generalization, Style Code, Content Map

## 1. Introduction

Medical image segmentation is critical for computer-aided diagnosis. Driven by large and diverse annotated datasets, deep learning-based segmentation models have achieved remarkable progress (Ronneberger et al., 2015; Milletari et al., 2016). However, data distribution mismatches (*a.k.a.*, domain shifts), caused by diverse imaging protocols, equipment vendors, or patient populations, *etc.*, between source (training) and target (testing) domains

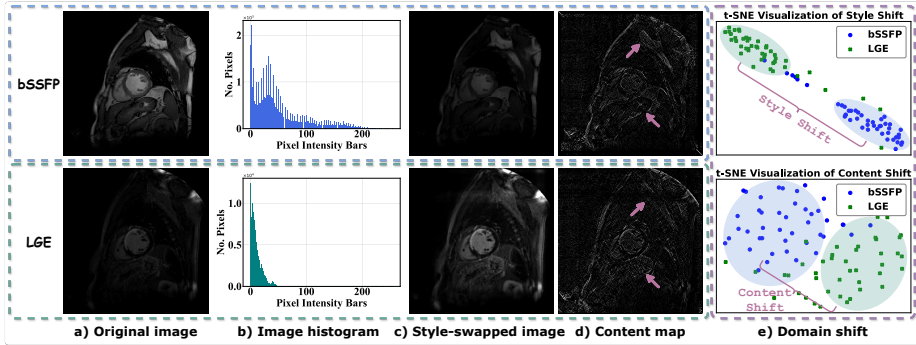


Figure 1: Illustration of style codes and content maps for bSSFP and LGE MRI sequences: a) original images showing disparities in both style (global image appearance) and content (local anatomical structures), b) image histograms reflecting domain shifts in terms of pixel intensities, c) style-swapped images generated by swapping the two original images’ style codes (top: bSSFP image with LGE style; bottom: LGE image with bSSFP style), d) content maps of the original images, and e) t-SNE (Van der Maaten and Hinton, 2008) visualization of domain shifts (top: style shift; bottom: content shift).

hinder the generalizability of trained models for clinical deployment (Castro et al., 2020; Zhou et al., 2022; Guan and Liu, 2021).

Domain generalization (DG) aims to mitigate domain shifts by training models on source-domain data and generalizing them to unseen target domains. Existing DG studies generally promote the learning of domain-invariant representations through two major paradigms: representation learning (Chen et al., 2019, 2020; Pei et al., 2021; Peng et al., 2022; Gao et al., 2022, 2023) and data augmentation (*a.k.a.*, domain randomization) (Ouyang et al., 2022; Zhou et al., 2021; Chen et al., 2023, 2025; Gu et al., 2023; Yang and Soatto, 2020; Xu et al., 2021a; Li et al., 2023). The former explicitly explores domain-invariant information via deterministic (Chen et al., 2019, 2020; Pei et al., 2021) or statistical (Gao et al., 2022, 2023) modeling. Although such methods yield intuitive decoupled features on source-domain data, their reliance on domain-specific training often hinders the generalization of disentanglement capabilities across different domains. In contrast, data augmentation-based DG methods alleviate this limitation by expanding the source-domain data distribution and thus implicitly encouraging models to excavate domain-invariant features. As a result, this paradigm has become the mainstream approach in the field. Specifically, these methods typically employ techniques such as Fourier transformation (Yang and Soatto, 2020; Xu et al., 2021a; Li et al., 2023), random convolution (Xu et al., 2021b; Ouyang et al., 2022; Choi et al., 2023), and feature statistics editing (Zhou et al., 2021; Chen et al., 2023, 2025), *etc* to achieve style augmentation on source-domain data. However, the underlying components involved in medical images remain underexplored. Modeling these components can provide valuable insights into the nature of domain shifts and guide the design of more effective data augmentation strategies.

To bridge this gap, we introduce a style–content decomposition strategy that decomposes an image into *style codes* and *content maps*, revealing that 1) the style code captures global image characteristics within a given anatomical structure and 2) the content maps describe the image’s anatomical structure. Fig. 1(c-d) visualizes style-swapped images (obtained by exchanging the style codes between two images) and content maps. It can be observed that the content maps delineate the anatomical structures of the original bSSFP and LGE images, while the style-swapped images exchange appearance between domains but preserve the original anatomical structures. Furthermore, the shift observed in the style codes is more significant than that in the content maps [Fig. 1(e)], as global variations in image characteristics are generally greater than local differences in anatomical structures. Based on these observations, we categorize domain shifts in medical images into two components: 1) **style shifts** (global image property variations) as indicated by deviations in the style codes, and 2) **content shifts** (local anatomical structure discrepancies) as reflected in differences between the content maps. Since quantitatively measuring and reducing these two types of shifts is infeasible without access to target domain data during training, we instead perturb the “style” and “content” components of source domain images to generate augmented images from diverse domains (simulating patients undergoing different imaging systems), enabling the training of a well-generalized medical image segmentation model.

To this end, we propose a **style content** decomposition-based data **augmentation** algorithm (**StyCona**) to advance domain generalizable medical image segmentation. Specifically, StyCona performs perturbations on the “style” (global image characteristics) and “content” (local anatomical structures) of an image by 1) blending style codes and 2) mixing content maps, respectively. StyCona generates augmented images with diverse styles and contents while preserving their semantic information, enabling the simulation of images from a wide range of domains for training a well-generalized segmentation model. We evaluate StyCona on cross-domain cardiac magnetic resonance imaging (MRI) segmentation and optic cup (OC)/optic disk (OD) fundus photography segmentation tasks. Experimental results demonstrate that StyCona is a promising solution for domain generalizable medical image segmentation.

Our main contributions can be summarized as follows:

- We propose a style–content decomposition strategy to model the underlying components of medical images and provide a deep insight into domain shifts.
- We propose StyCona, a novel data augmentation algorithm for domain generalizable medical image segmentation. StyCona can be easily integrated into off-the-shelf medical image segmentation backbones and effectively mitigates domain shifts.
- StyCona leads to state-of-the-art performance across a wide range of tasks and provides a compelling alternative to Fourier transformation-based, random convolution-based, and feature statistics editing-based domain generalization methods.

## 2. Methodology

For a domain generalizable medical image segmentation task, the training set can be denoted as  $\mathcal{D} = \{\mathcal{S}_k | \mathcal{S}_k = \{(x_{i(k)}, y_{i(k)})_{i=1}^{N_k}\}_{k=1}^K\}$ , where  $x_{i(k)}$  represents the  $i^{th}$  image in the  $k^{th}$

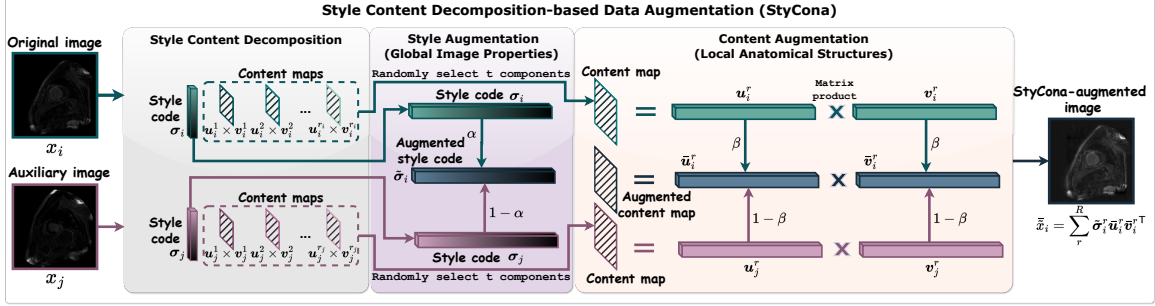


Figure 2: Schematic diagram of the proposed **style content** decomposition-based data augmentation algorithm (**StyCona**). StyCona includes three steps: 1) style content decomposition, 2) style augmentation, and 3) content augmentation.  $x_i$  and  $x_j$  represent original images, and  $\tilde{x}$  denotes a StyCona-augmented sample.

domain and  $y_{i(k)}$  is its corresponding ground truth segmentation label. This paper focuses on the most challenging single-source domain generalization setting (*i.e.*,  $K = 1$ ), in which the segmentation model  $f(\cdot; \theta)$  is trained on a single source domain and evaluated on one or more unseen target domains. Note that we omit the domain index for brevity.

## 2.1. Style Content Decomposition-based Data Augmentation (StyCona)

Domain shifts in medical images can be characterized two principal components: 1) **"style"** shifts, referring to *global* variations in image properties such as illumination, contrast, and color; and 2) **"content"** shifts, which involve *local* changes in image characteristics and are usually associated with differences in the visibility of specific tissues. Based on this assumption, we propose StyCona to mitigate both style and content shifts through corresponding style and content augmentations. As illustrated in Fig. 2, StyCona mainly includes three steps: 1) style content decomposition, 2) style augmentations, and 3) content augmentation. Specifically, the style-content decomposition is performed using singular value decomposition (SVD) (Klema and Laub, 1980), which factorizes an image into its **singular values (style codes)** and **rank-one matrices (content maps)**. Then, the style and content augmentations are achieved by perturbing the style codes and content maps, respectively.

### 2.1.1. STYLE CONTENT DECOMPOSITION

Low-rank matrices of an image correspond to its principal components (Abdi and Williams, 2010; Candès et al., 2011). Based on this idea, prior work has employed rank-one matrices as the principal parts of an image for restoration tasks (Gao and Zhuang, 2020). We leverage SVD to show that an image's singular values encode its **style codes**, while the associated

rank-one matrices represent its **content maps**:

$$x = \sum_{r=1}^R \underbrace{\sigma^r}_{style\ code} \underbrace{\mathbf{u}^r \mathbf{v}^{r\top}}_{content\ map} \quad (1)$$

where  $R$  denotes the rank of the image, corresponding to the number of non-zero singular values. SVD provides the optimal rank-one decomposition in the least-squares sense. It guarantees that the set  $\Phi = \{\mathbf{u}^1 \mathbf{v}^{1\top}, \mathbf{u}^2 \mathbf{v}^{2\top}, \dots, \mathbf{u}^R \mathbf{v}^{R\top}\}$  forms a complete basis for the column and row spaces of  $x$ .

- **Content Map.** Each rank-one matrix in  $\Phi$  functions as a basis pattern of the image, and any image structure can be represented as a linear combination of these patterns. Thus,  $\Phi$  completely defines the anatomical structures of the image.
- **Style Code.** Each scalar  $\sigma^r$  acts as a global multiplier for the corresponding basis pattern  $(\mathbf{u}^r \mathbf{v}^{r\top})$ . It modulates the magnitude of pixel intensity in the image, scaling the values of the basis pattern proportionally.

As illustrated in Fig. 1, swapping the style codes of the bSSFP and LGE images results in style transfer between them, while summing all content maps of one of the images reconstructs its complete anatomical structure.

### 2.1.2. STYLE AUGMENTATION

Style augmentation aims to alleviate style shifts (global variations in image properties). As depicted in Fig. 2, we perform style augmentation on an image  $x_i$  by blending its **style codes** with those of an auxiliary image  $x_j$  in an element-wise manner:

$$\tilde{\sigma}_i^r = \alpha \times \sigma_i^r + (1 - \alpha) \times \sigma_j^r \quad (2)$$

where the weight  $\alpha \sim U(0, 1)$  controls the mix strength,  $\sigma_i^r$  represents the  $r_{th}$  singular value of image  $x_i$ , and  $i/j$  indicates the sample index ( $i \neq j$ ).

### 2.1.3. CONTENT AUGMENTATION

We devise content augmentation to mitigate content shifts (local disparities in anatomical structure). This is achieved by mixing a set of  $t$  randomly selected **content maps** from an image  $x_i$  with another set of  $t$  randomly selected content maps from an auxiliary image  $x_j$  [Fig. 2]. The perturbation to each content map is formulated as:

$$\tilde{\mathbf{u}}_i^r = \beta \times \mathbf{u}_i^r + (1 - \beta) \times \mathbf{u}_j^r \quad or \quad \tilde{\mathbf{v}}_i^r = \beta \times \mathbf{v}_i^r + (1 - \beta) \times \mathbf{v}_j^r \quad (3)$$

where the weight  $\beta \sim U(0, 1)$  and  $\mathbf{u}_{i/j}^r / \mathbf{v}_{i/j}^r$  represents the left/right singular vector of image  $x_{i/j}$ .

In a nutshell, StyCona performs style and content augmentation by Eq. (1)(2)(3), and generates an augmented image as  $\tilde{x}_i = \sum_{r=1}^R \tilde{\sigma}_i^r \tilde{\mathbf{u}}_i^r \tilde{\mathbf{v}}_i^{r\top}$ .

#### 2.1.4. LOSS SUPERVISION

Afterwards, we formulate the segmentation loss  $\mathcal{L}$  for training a domain generalizable model  $f(\cdot; \theta)$  based on StyCona augmented images:

$$\mathcal{L} = \frac{1}{N} \sum_i^N \mathcal{L}_{seg}(f(\bar{x}_i, \theta), y_i) \quad (4)$$

where  $\mathcal{L}_{seg}$  denotes a segmentation criterion.

### 3. Experiments and Results

**Cross-Domain Cardiac Magnetic Resonance Imaging (MRI) Segmentation** The MS-CMR Dataset (*Single Source and Single Target Domain*) dataset (Zhuang, 2018) contains 45 subjects, each with bSSFP and LGE MRI sequences, along with ground truth annotations for the right ventricle (RV), left ventricle (LV), and myocardium (MYO). All images are normalized to the range  $[0, 1]$  and resampled to a uniform resolution of  $1.0 \times 1.0$  mm. This experimental setting evaluates a segmentation model’s ability to generalize across MRI sequences for cardiac structure segmentation, specifically from LGE to bSSFP and vice versa. For each direction, one sequence (*e.g.*, bSSFP) is treated as the source domain and is divided into training and validation sets with a 8 : 2 ratio, while another sequence (*e.g.*, LGE) serves as the target domain and is used solely for testing.

**Cross-Domain Optic Cup (OC) and Optic Disc (OD) Fundus Image Segmentation** The Fundus Image Benchmark (*Single Source and Multiple Target Domains*) (Chen et al., 2023) is established based on the ORIGA (Zhang et al., 2010), Drishti-GS (Sivaswamy et al., 2014), REFUGE (Orlando et al., 2020), and RIGA (Almazroa et al., 2018) (BinRushed and Magribia) datasets. This setting evaluates the model’s generalization capability for the joint OC and OD segmentation across multiple target domains. The ORIGA dataset is used as the source domain with the training and validation split following TriD (Chen et al., 2023); the other datasets (BinRushed, Drishti-GS, Magribia, and REFUGE) act as target domains for cross-domain evaluation.

**Implementation Details.** We conducted the experiments using PyTorch (Paszke et al., 2019) on an NVIDIA A40 GPU with 48G GPU memory. All compared methods were optimized using an AdamW optimizer (Kingma and Ba, 2015) with a fixed learning rate of  $1e - 4$  during the 100 training epochs for both the cardiac MRI and fundus image segmentation tasks. U-Net (Ronneberger et al., 2015) was employed as the baseline segmentation model. The combination of cross-entropy and Dice loss (Milletari et al., 2016) was used as the segmentation criterion. All images were resized to  $256 \times 256$  for both training and testing, and the predicted labels were rescaled to their original resolutions for evaluation. We set the number of perturbed content maps  $t = 16$  (please refer to Section 3.2.2 for further analysis).

#### 3.1. Comparison with State of the Arts

We compared StyCona with state-of-the-art DG methods: 1) Fourier transformation-based: amplitude swap (AmpSwap) (Yang and Soatto, 2020), amplitude mixup (AmpMix) (Xu

et al., 2021a), and FMAug (Li et al., 2023)); 2) Feature statistics editing-based: MixStyle (Zhou et al., 2021), TriD (Chen et al., 2023), and ConStyX (Chen et al., 2025); 3) Random convolution-based: RandConv (Xu et al., 2021b), CIDA (Ouyang et al., 2022), and PRandConv (Choi et al., 2023). We re-implemented all the compared methods in a unified experimental setup for fair comparison. All the methods are built upon the same baseline segmentation model (U-Net). In general, StyCona sets the state-of-the-art in all three settings, both quantitatively [Table 1 and Table 2] and qualitatively [Fig. 3], showcasing its superiority in domain generalizable medical image segmentation.

### 3.1.1. RESULTS ON CARDIAC MRI

As reported in Table 1, StyCona achieves consistent performance improvements over the compared methods in the cardiac MRI segmentation task. In general, almost all the compared methods surpass the baseline model, indicating their effectiveness in addressing domain shifts. However, it is worth noting that some methods, *e.g.*, AmpMix (Xu et al., 2021a) and TriD (Chen et al., 2023), yield segmentation results inferior to those of the baseline model in the bSSFP  $\rightarrow$  LGE scenario. This may result from the fact that the blended amplitude spectrum in AmpMix and the mixed feature statistics in TriD generate style-augmented images that are insufficient for mitigating content shifts, resulting in the models overfitting spurious correlations between the augmented images and their corresponding segmentation labels. In contrast, StyCona demonstrates a clear advantage in handling both style and content shifts by style content augmentation. These results validate the key idea of StyCona and highlight its effectiveness in domain generalizable medical image segmentation.

### 3.1.2. RESULTS ON FUNDUS IMAGE

We further evaluate StyCona in a single-source, multi-target domain setting. As shown in Table 2, all methods generally achieve comparable average performance across the four target domains. However, the two random convolution-based approaches (*i.e.*, CIDA (Ouyang et al., 2022) and PRandConv (Choi et al., 2023)) yield relatively unsatisfactory results. This may be attributed to that the random convolution operations produce augmented images with distorted content that is inconsistent with the corresponding segmentation labels, thus misleading the segmentation models during training. In contrast, StyCona shows more robust performance across the four target domains, obtaining the highest average DSC and competitive ASD. These results further suggest the effectiveness of StyCona in domain generalizable medical image segmentation with multiple target domains.

### 3.1.3. QUALITATIVE RESULTS.

As shown in Fig. 3, StyCona produces segmentation results with more precise object delineation. The improvement can be attributed to StyCona’s style and content augmentations, which enable the augmented samples to cover a wide range of unseen domains, thereby allowing the trained model to generate accurate segmentation maps for unseen data. In comparison, methods such as AmpMix (Xu et al., 2021a), MixStyle (Zhou et al., 2021), and PRandConv (Choi et al., 2023) yield relatively unsatisfactory results. AmpMix and MixStyle rely solely on style augmentation by blending amplitude spectra and adjusting

Table 1: Comparison with state-of-the-art methods on the cross-domain cardiac MRI segmentation task (single target domain). The best and second-best results are highlighted in **bold** and underline, respectively.

Method	bSSFP $\rightarrow$ LGE		LGE $\rightarrow$ bSSFP	
	DSC $\uparrow$	ASD $\downarrow$	DSC $\uparrow$	ASD $\downarrow$
U-Net (Ronneberger et al., 2015)	65.97	6.55	76.91	3.41
AmpSwap (Yang and Soatto, 2020)	70.93	6.48	78.74	3.26
AmpMix (Xu et al., 2021a)	63.89	6.44	80.07	2.46
FMAug (Li et al., 2023)	<u>72.46</u>	13.67	80.54	2.57
MixStyle (Zhou et al., 2021)	69.26	10.91	80.81	<u>2.69</u>
TriD (Chen et al., 2023)	65.12	10.25	79.14	4.60
ConStyX (Chen et al., 2025)	68.63	7.89	<u>81.30</u>	2.85
RandConv (Xu et al., 2021b)	71.90	<u>5.65</u>	75.17	4.27
CIDA (Ouyang et al., 2022)	69.72	8.63	72.85	4.61
PRandConv (Choi et al., 2023)	56.61	8.75	75.57	3.38
StyCona (ours)	<b>73.39</b>	<b>4.33</b>	<b>81.59</b>	<b>2.24</b>

Table 2: Comparison with state-of-the-art methods on the fundus image segmentation tasks (Source: ORIGA; Target: REFUGE, Drishti-GS, BinRushed, and Magribia). The best and second-best results are highlighted in **bold** and underline, respectively.

Method	BinRushed		Drishti-GS		Magribia		REFUGE		Average	
	DSC (%) $\uparrow$	ASD $\downarrow$								
U-Net (Ronneberger et al., 2015)	54.82	7.07	77.99	1.16	61.19	8.10	79.49	1.89	68.37	4.56
AmpSwap (Yang and Soatto, 2020)	63.56	4.36	78.16	1.13	<u>66.13</u>	<u>4.45</u>	<u>81.84</u>	<u>1.45</u>	72.41	<u>2.85</u>
AmpMix (Xu et al., 2021a)	65.08	<u>4.32</u>	77.06	1.09	<b>68.14</b>	<b>4.29</b>	79.50	1.67	72.44	<b>2.84</b>
FMAug (Li et al., 2023)	63.79	5.03	78.34	<u>1.04</u>	64.33	7.28	<b>82.17</b>	<b>1.29</b>	72.16	3.66
MixStyle (Zhou et al., 2021)	63.95	4.72	<u>80.36</u>	1.06	63.97	6.04	81.93	1.45	72.55	3.32
TriD (Chen et al., 2023)	<u>66.27</u>	4.34	77.08	1.24	65.42	4.53	79.36	1.57	72.03	2.92
ConStyX (Chen et al., 2025)	62.91	5.99	<b>80.69</b>	<b>1.03</b>	64.47	7.16	80.15	1.85	72.05	4.01
RandConv (Xu et al., 2021b)	63.75	4.70	79.35	1.13	65.61	5.07	81.52	1.46	<u>72.56</u>	3.09
CIDA (Ouyang et al., 2022)	53.16	11.34	78.55	5.18	51.27	14.61	68.09	6.62	62.76	8.44
PRandConv (Choi et al., 2023)	44.60	9.84	75.23	1.48	53.34	8.68	76.61	2.57	62.44	5.64
StyCona (ours)	<b>67.80</b>	<b>3.60</b>	78.43	1.08	65.71	4.37	80.68	1.49	<b>73.16</b>	2.63

the mean and standard deviation of samples, respectively. Meanwhile, the effectiveness of PRandConv is limited by its progressively applied random convolutions, which generate content-distorted images and fail to adequately alleviate variations in anatomical structures. These qualitative results, consistent with the quantitative performance, further suggest the effectiveness of our approach.

### 3.2. Ablation Study

#### 3.2.1. EFFECTIVENESS OF EACH COMPONENT

In Table 3, we present ablation experiments to analyze the contributions of each component of StyCona. These experiments were conducted under the cardiac MRI segmentation task. The results reveal a consistent trend: segmentation performance improves as the proposed style and content augmentation components are gradually integrated into our method. Specifically, the baseline model (*i.e.*, U-Net) performs relatively unsatisfactorily on the target domain, as it tends to learn domain-specific decision rules based on source domain data.

Image	Baseline	AmpSwap	AmpMix	FMAug	MixStyle	TriD	ConStyX	RandConv	CIDA	PRandConv	Ours	Ground Truth	
bSSFP → LGE	✗	✗	✗	✗	✗	✗	✗	✗	✗	✗	✗	✗	
LGE → bSSFP	✗	✗	✗	✗	✗	✗	✗	✗	✗	✗	✗	✗	
ORIGA → BinRushed													
ORIGA → Drishti-GS													
ORIGA → Magravia													
ORIGA → REFUGE													

Figure 3: Qualitative results on the cardiac MRI segmentation and the OC/OD fundus image segmentation tasks.

Then, the segmentation performance increases by a large gap when the style augmentation operation is introduced for effectively mitigating style shifts, which are an essential part of domain shifts in these scenarios. In contrast, the improvement is more significant, with an increase of over 7% in DSC, when only the content augmentation component is introduced to address the content shifts, another key aspect of domain shifts. Finally, by incorporating both the style and content augmentation modules to address global variations in image appearance and local differences in anatomical structures, our final method achieves the best performance with DSC of 73.39% and 81.59% on the bSSFP → LGE and LGE → bSSFP scenarios, respectively. This result demonstrates the effectiveness of each component and validates our assumptions of the style content decomposition and the corresponding style and content augmentation to alleviate the domain shifts.

### 3.2.2. IMPACT OF NO. PERTURBED CONTENT MAPS

According to Eq. (1)(2)(3), perturbing the style codes alters only an image’s style without changing its semantic information corresponding to segmentation labels. On the other hand, perturbing  $t$  randomly selected content maps results in changes in local anatomical structures (*e.g.*, background tissues or target object-related boundaries), which is the goal of StyCona to enhance the robustness of segmentation models to local anatomical structure variations. Qualitatively, Fig. 4(a) shows the StyCona-augmented samples with varying numbers of perturbed content maps ( $t = 8, 16, 32$ ). Compared with the original images, the augmented images with  $t = 8, 16$  exhibit variations in global image appearance and local anatomical structures while remaining consistent with the ground truth segmentation labels. In contrast, excessive perturbation is introduced into some target boundaries when  $t = 32$ , which may alter their ground truth labels. Quantitatively,  $t = 16$  yields the highest

Table 3: Ablation study of StyCona on the cross-sequence setting. The best results are highlighted in **bold**.

Method	StyCona		bSSFP $\rightarrow$ LGE		LGE $\rightarrow$ bSSFP	
	Style augmentation	Content augmentation	DSC $\uparrow$	ASD $\downarrow$	DSC $\uparrow$	ASD $\downarrow$
Baseline			65.97	6.55	76.91	3.41
Baseline + Style	✓		68.98	3.20	80.45	2.40
Baseline + Content		✓	72.31	5.16	81.17	2.43
Baseline + Style + Content	✓	✓	<b>73.39</b>	<b>4.33</b>	<b>81.59</b>	<b>2.24</b>

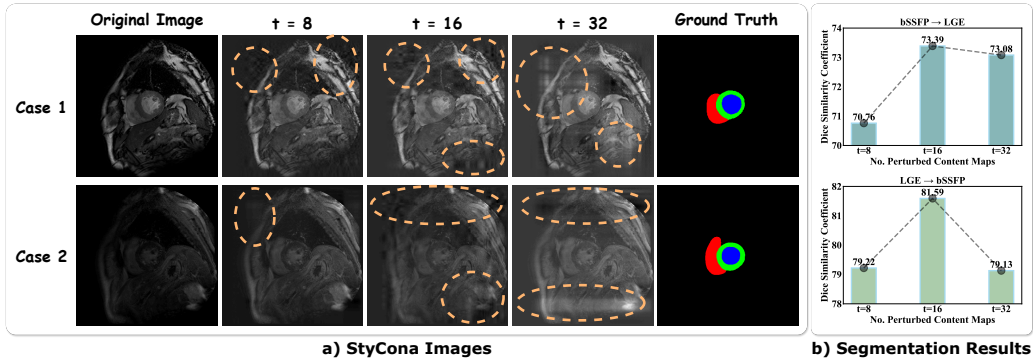


Figure 4: Illustration of a) StyCona-augmented images with different numbers of perturbed content maps ( $t = 8$ ,  $t = 16$ , and  $t = 32$ ) for two randomly selected original images (The orange dashed circles highlight some content-perturbed regions) and b) Segmentation results for  $t = 8$ ,  $t = 16$ , and  $t = 32$  on cardiac MRI segmentation.

DSC in both the bSSFP  $\rightarrow$  LGE and LGE  $\rightarrow$  bSSFP scenarios. Based on these results, we set  $t = 16$  in StyCona to balance perturbation strength with the invariance of segmentation labels, ensuring label consistency after content augmentation.

## 4. Conclusion

We propose StyCona, a novel data augmentation algorithm for domain generalizable medical image segmentation. Our style content decomposition strategy reveals that an image’s singular values function as style codes, governing its global image properties, while its rank-one matrices serve as content maps, determining its anatomical structures. Based on this decomposition, we categorize domain shifts into style and content shifts *w.r.t.* deviations in style codes and content maps, respectively. Then, StyCona perturbs style codes for style augmentation and blends content maps for content augmentation, addressing both types of domain shifts accordingly. Extensive experiments on cardiac MRI segmentation with a single target domain and fundus image segmentation with multiple target domains demonstrate that StyCona is an effective data augmentation technique for domain-generalizable medical image segmentation.

## References

Hervé Abdi and Lynne J Williams. Principal component analysis. *Wiley interdisciplinary reviews: computational statistics*, 2(4):433–459, 2010.

Ahmed Almazroa, Sami Alodhayb, Essameldin Osman, Eslam Ramadan, Mohammed Humadi, Mohammed Dlaim, Muhannad Alkatee, Kaamran Raahemifar, and Vasudevan Lakshminarayanan. Retinal fundus images for glaucoma analysis: the riga dataset. In *Medical Imaging 2018: Imaging Informatics for Healthcare, Research, and Applications*, volume 10579, pages 55–62. SPIE, 2018.

Emmanuel J Candès, Xiaodong Li, Yi Ma, and John Wright. Robust principal component analysis? *Journal of the ACM (JACM)*, 58(3):1–37, 2011.

Daniel C Castro, Ian Walker, and Ben Glocker. Causality matters in medical imaging. *Nature Communications*, 11(1):3673, 2020.

Cheng Chen, Qi Dou, Hao Chen, Jing Qin, and Pheng-Ann Heng. Synergistic image and feature adaptation: Towards cross-modality domain adaptation for medical image segmentation. In *Proceedings of the AAAI conference on artificial intelligence*, volume 33, pages 865–872, 2019.

Cheng Chen, Qi Dou, Hao Chen, Jing Qin, and Pheng Ann Heng. Unsupervised bidirectional cross-modality adaptation via deeply synergistic image and feature alignment for medical image segmentation. *IEEE transactions on medical imaging*, 39(7):2494–2505, 2020.

Xi Chen, Zhiqiang Shen, Peng Cao, Jinzhu Yang, and Osmar R Zaiane. Constyx: Content style augmentation for generalizable medical image segmentation. In *International Conference on Medical Image Computing and Computer-Assisted Intervention*, pages 100–110. Springer, 2025.

Ziyang Chen, Yongsheng Pan, Yiwen Ye, Hengfei Cui, and Yong Xia. Treasure in distribution: a domain randomization based multi-source domain generalization for 2d medical image segmentation. In *International Conference on Medical Image Computing and Computer-Assisted Intervention*, pages 89–99. Springer, 2023.

Seokeon Choi, Debasmit Das, Sungha Choi, Seunghan Yang, Hyunsin Park, and Sungrock Yun. Progressive random convolutions for single domain generalization. In *Proceedings of the IEEE/CVF Conference on Computer Vision and Pattern Recognition*, pages 10312–10322, 2023.

Shangqi Gao and Xiahai Zhuang. Rank-one network: An effective framework for image restoration. *IEEE Transactions on Pattern Analysis and Machine Intelligence*, 44(6):3224–3238, 2020.

Shangqi Gao, Hangqi Zhou, Yibo Gao, and Xiahai Zhuang. Joint modeling of image and label statistics for enhancing model generalizability of medical image segmentation. In *International Conference on Medical Image Computing and Computer-Assisted Intervention*, pages 360–369. Springer, 2022.

Shangqi Gao, Hangqi Zhou, Yibo Gao, and Xiahai Zhuang. Bayeseg: Bayesian modeling for medical image segmentation with interpretable generalizability. *Medical Image Analysis*, 89:102889, 2023.

Ran Gu, Guotai Wang, Jiangshan Lu, Jingyang Zhang, Wenhui Lei, Yinan Chen, Wenjun Liao, Shichuan Zhang, Kang Li, Dimitris N Metaxas, et al. Cddsa: Contrastive domain disentanglement and style augmentation for generalizable medical image segmentation. *Medical Image Analysis*, 89:102904, 2023.

Hao Guan and Mingxia Liu. Domain adaptation for medical image analysis: a survey. *IEEE Transactions on Biomedical Engineering*, 69(3):1173–1185, 2021.

Diederik P Kingma and Jimmy Ba. Adam: A method for stochastic optimization. In *International Conference on Learning Representations*, 2015.

Virginia Klema and Alan Laub. The singular value decomposition: Its computation and some applications. *IEEE Transactions on automatic control*, 25(2):164–176, 1980.

Heng Li, Haojin Li, Wei Zhao, Huazhu Fu, Xiuyun Su, Yan Hu, and Jiang Liu. Frequency-mixed single-source domain generalization for medical image segmentation. In *International Conference on Medical Image Computing and Computer-Assisted Intervention*, pages 127–136. Springer, 2023.

Fausto Milletari, Nassir Navab, and Seyed-Ahmad Ahmadi. V-net: Fully convolutional neural networks for volumetric medical image segmentation. In *2016 fourth international conference on 3D vision (3DV)*, pages 565–571. Ieee, 2016.

José Ignacio Orlando, Huazhu Fu, João Barbosa Breda, Karel Van Keer, Deepti R Bathula, Andrés Diaz-Pinto, Ruogu Fang, Pheng-Ann Heng, Jeyoung Kim, JoonHo Lee, et al. Refuge challenge: A unified framework for evaluating automated methods for glaucoma assessment from fundus photographs. *Medical image analysis*, 59:101570, 2020.

Cheng Ouyang, Chen Chen, Surui Li, Zeju Li, Chen Qin, Wenjia Bai, and Daniel Rueckert. Causality-inspired single-source domain generalization for medical image segmentation. *IEEE Transactions on Medical Imaging*, 42(4):1095–1106, 2022.

Adam Paszke, Sam Gross, Francisco Massa, Adam Lerer, James Bradbury, Gregory Chanan, Trevor Killeen, Zeming Lin, Natalia Gimelshein, Luca Antiga, et al. Pytorch: An imperative style, high-performance deep learning library. *Advances in neural information processing systems*, 32, 2019.

Chenhao Pei, Fuping Wu, Liqin Huang, and Xiahai Zhuang. Disentangle domain features for cross-modality cardiac image segmentation. *Medical Image Analysis*, 71:102078, 2021.

Linkai Peng, Li Lin, Pujin Cheng, Ziqi Huang, and Xiaoying Tang. Unsupervised domain adaptation for cross-modality retinal vessel segmentation via disentangling representation style transfer and collaborative consistency learning. In *2022 IEEE 19th International Symposium on Biomedical Imaging (ISBI)*, pages 1–5. IEEE, 2022.

Olaf Ronneberger, Philipp Fischer, and Thomas Brox. U-net: Convolutional networks for biomedical image segmentation. In *Medical image computing and computer-assisted intervention–MICCAI 2015: 18th international conference, Munich, Germany, October 5–9, 2015, proceedings, part III* 18, pages 234–241. Springer, 2015.

Jayanthi Sivaswamy, SR Krishnadas, Gopal Datt Joshi, Madhulika Jain, and A Ujjwaft Syed Tabish. Drishti-gs: Retinal image dataset for optic nerve head (ohn) segmentation. In *2014 IEEE 11th international symposium on biomedical imaging (ISBI)*, pages 53–56. IEEE, 2014.

Laurens Van der Maaten and Geoffrey Hinton. Visualizing data using t-sne. *Journal of machine learning research*, 9(11), 2008.

Qinwei Xu, Ruipeng Zhang, Ya Zhang, Yanfeng Wang, and Qi Tian. A fourier-based framework for domain generalization. In *Proceedings of the IEEE/CVF Conference on Computer Vision and Pattern Recognition*, pages 14383–14392, 2021a.

Zhenlin Xu, Deyi Liu, Junlin Yang, Colin Raffel, and Marc Niethammer. Robust and generalizable visual representation learning via random convolutions. In *International Conference on Learning Representations*, 2021b.

Yanchao Yang and Stefano Soatto. Fda: Fourier domain adaptation for semantic segmentation. In *Proceedings of the IEEE/CVF conference on computer vision and pattern recognition*, pages 4085–4095, 2020.

Zhuo Zhang, Feng Shou Yin, Jiang Liu, Wing Kee Wong, Ngan Meng Tan, Beng Hai Lee, Jun Cheng, and Tien Yin Wong. Origalight: An online retinal fundus image database for glaucoma analysis and research. In *2010 Annual international conference of the IEEE engineering in medicine and biology*, pages 3065–3068. IEEE, 2010.

Kaiyang Zhou, Yongxin Yang, Yu Qiao, and Tao Xiang. Domain generalization with mixstyle. In *International Conference on Learning Representations*, 2021.

Kaiyang Zhou, Ziwei Liu, Yu Qiao, Tao Xiang, and Chen Change Loy. Domain generalization: A survey. *IEEE Transactions on Pattern Analysis and Machine Intelligence*, 45(4): 4396–4415, 2022.

Xiahai Zhuang. Multivariate mixture model for myocardial segmentation combining multi-source images. *IEEE transactions on pattern analysis and machine intelligence*, 41(12): 2933–2946, 2018.